Applied Magnetic Resonance (2020) 51:1005–1017
https://doi.org/10.1007/s00723-020-01222-0

Applied
Magnetic Resonance

ORIGINAL PAPER

Fine Analysis of the Structure and Dynamics of Vanadyl Complexes Adsorbed on TiO_2 (Anatase) Surface: EPR Investigation

Anatoly I. Kulak[1] · Sergey O. Travin[2] · Alexander I. Kokorin[2,3]

Received: 1 June 2020 / Revised: 8 July 2020 / Published online: 28 August 2020

Abstract
This work continues EPR investigation of photocatalytic systems based on vanadium modified titanium dioxide (anatase) surface containing various concentrations of VO^{2+} paramagnetic centers (PCs). Three different types of the isolated PCs are revealed on the surface of V–TiO_2 nanoparticles and quantitatively characterized. Time-dependent transitions among these PCs were observed and kinetic behavior was described using new theoretical approach and the developed numerical calculation procedure. The slow-process kinetic rate constant has been calculated from EPR data.

1 Introduction

Vanadium doping of titanium dioxide has been studied in detail in many works with the aim to increase photocatalytic activity and for enlarging the area of spectral sensitivity to the visible light region in processes of photodegradation of dyes [1–5], different organic compounds (ethanol, ethene, formic acid) [6–9], chlorinated hydrocarbons [10], NO_2, NO_x [11, 12]. Besides, an interest to V-doped TiO_2 is connected with perspectives of its application as the heterogeneous catalyst [13–17], electrochromic [18, 19], photochromic [20], and ferromagnetic [21] materials, as an electrode material for electrocatalytic oxidative processes [22] and electrochemical nitrogen reduction [23], in lithium- and sodium-ionic batteries [24], photovoltaic cells [25], and in redox-sensors [26].

✉ Anatoly I. Kulak
kulak@igic.bas-net.by

[1] Institute of General and Inorganic Chemistry, National Academy of Sciences of Belarus, Surganov Str. 9/1, 220072 Minsk, Belarus

[2] N.N. Semenov Federal Research Center for Chemical Physics, Russian Academy of Sciences, Moscow, Russian Federation

[3] Plekhanov Russian University of Economics, Moscow, Russian Federation

The analysis of published data evidences about complex and in some cases non-certain dependence of functional properties of V-doped TiO_2 on concentration of doped or adsorbed vanadium, on the method of modification and regimes of further treatment. As an example, studying photocatalytic activity of V-doped TiO_2, some authors showed the maximum increase of the activity at vanadium content between 0.002 and 0.05 mol% [1–3] while others declared much higher concentrations [4, 6, 8, 10]. Also, strong influence on photocatalytic behavior causes a method of preparation: impregnation, sol–gel, implantation of vanadium ions, etc., and connected with them differences in either adsorbed forms (ions or complexes) or ions incorporated into crystalline lattice, or as V_2O_5 nanoclusters forming micro- or nanoheterogeneous systems.

In the previous paper we have demonstrated that using surface modification of TiO_2 by adsorbing vanadyl VO^{2+} ions from aqueous solutions, one of the main reasons of such influence is the formation of various types the vanadyl-ion complexes with the titanium dioxide matrix [27]. Comparing dependences of the photocatalytic activity of the samples with different VO^{2+} content with the analogous plots of isolated and aggregated paramagnetic centers, PCs, it was concluded that catalytically active are the most probably the isolated vanadyl centers on the V-doped TiO_2 surface [27]. Such unique information concerning peculiarities of the structure, spatial organization and properties of vanadium ions on TiO_2 surface could be obtained only with the use of the electron paramagnetic resonance (EPR) technique.

Taking into consideration written above, the aim of this work was the detailed analysis of structural peculiarities and dynamics of reorganization of vanadyl complexes formed on TiO_2 (anatase) surface using CW X-band EPR technique.

2 Experimental

2.1 Substances and Sample Preparation

All preparation procedures were quite similar to those described in our previous paper in details [27]. Shortly, adsorption of vanadyl ions onto TiO_2 surface was performed by a 2 h treatment of commercially available pure anatase (Hombikat UV 100, Sachtleben Chemie, Germany) aqueous suspension containing a vanadium (IV) sulfate oxide $VOSO_4$ (99.9%, Alfa Aesar, Germany) additive in a variable concentration of 0.22 to 7.0 mmol/l. The suspension was shaken to attain equilibrium, and then, the V-doped TiO_2 powder was separated from the solution by centrifugation, washed twice with doubly distilled water by 5 min each and dried at 295 K during 24 h in air till the constant mass.

The BET surface area of pure Hombikat UV-100 sample was found *ca*. 295 ± 14 $m^2\ g^{-1}$ and dropped down to 198 ± 11 $m^2\ g^{-1}$ after wetting with distilled water followed by calcinations at 573 K for 60 min. It has been shown in [27] that the increase in the vanadium content by elevating concentration in impregnating $VOSO_4$ solution from 0.22 to 7.0 mmol dm^{-3} has resulted in $[VO^{2+}]$ surface concentrations from 0.57×10^{19} to 1.25×10^{20} spin/g and led to an increase in the specific surface

area to 203–209 $m^2\ g^{-1}$, which, however, is in the region of statistical dispersion of the experimental data.

The average weight of the samples prepared for EPR measurements was in the range of 40 ± 5 mg. For recording the spectrum of the whole paramagnetic staff in a powder, we have added 0.2 cm^3 of 1.0 ± 0.05 mol/dm^3 of the ascorbic acid (AA) solution in CH_3OH: $H_2O = 1{:}1$ mixture by volume into the ampoule using Hamilton microsyringe, and afterwards the ampoule was sealed. The solution impregnated the powder in 20–30 s and was ready for EPR spectra recording. Such "wet" samples were kept in the dark in a closed box during all time of the experiment. The procedure of adding AA to V-TiO_2 system was used for reducing the main part of the oxidized V^{5+} adsorbed ions to the paramagnetic V^{4+} state. Indeed, due to the wide band gap nature of semiconductor TiO_2, vanadium PCs formed from $VOSO_4$ on the titania surface are mainly at the oxidized, V^{5+}, electron configuration.

2.2 EPR Measurements

The EPR spectra were recorded using a CW Varian E-3 *X*–band spectrometer in quartz ampules of 3.0 mm inner diameter (from Bruker) at a microwave field frequency of 9.5 GHz, modulation frequency of 100 kHz, and microwave field power of 1.0 mW at 77 K in the presence of air. The *g*-factor of the samples was determined using a standard MgO sample containing Mn^{2+} ions as admixture. Spin-Hamiltonian parameters of VO^{2+} species were determined according to recommendations given in [28] based on the second-order amendments. The content of the paramagnetic centers (PCs) of the vanadium V^{4+} and VO^{2+} ions in the samples was determined by double integration of the spectra and comparison of the results with the data of the reference (the spectrum of the $CuCl_2{\cdot}2H_2O$ single crystal with a known number of spins). The experimental EPR spectra were processed using the computer Program package provided by Prof. A. Kh. Vorob'ev (Department of Chemistry, M. V. Lomonosov Moscow State University) [29]. All measuring data were inside the error limits range except those listed below.

2.3 Calculation Details

Since there was no a priori information about the reference EPR spectra of the material under investigation, we applied blind recognition to the processing of EPR spectra by establishing the most probable set of basis spectra and attributing the observed spectra to a linear decomposition on a selected basis. For this purpose, we created a set of linear algebraic transformations with data sets characterized by the identity of the set of abscises X_i (in our case—the magnetic field H). In fact, EPR spectra obtained at different times and in different conditions should provide the possibility of comparison and algebraic transformations of numerical arrays Y_i^k (Y is a signal at the i-th point of the k-spectrum) with the same X_i values. Since the H field values were obtained by digitizing an analog signal, the first task of data preprocessing was to convert primary arrays to a unified set of equidistant magnetic field values on the abscissa axis. At the same time, it was necessary to get rid of high-frequency noise,

which could lead to pseudo-revealing of false peaks. For this purpose, interpolation by B-splines was applied by smooth decomposition of the arbitrary function $s(x)$ by polynomials of N_i^k degree k of special kind determined recursively [30, 31]:

$$s(x) = \sum_{i=j-k}^{j} c_i N_i^{k+1} \tag{1}$$

To build up a spline, the grid of horizontal nodes was set, located so that inside the interval $[a, b]$ there are g nodes, and at the edges are $k+1$ nodes on each, where k is the degree of spline:

$$\lambda_0 = \lambda_1 = \cdots = \lambda_k = a; \lambda_{g+k+1} = \lambda_{g+k+2} = \cdots = \lambda_{g+2k+1} = b$$

$$\lambda_{k+i} = a + i \bullet h; \quad h = \frac{a-b}{g}; \quad 1 \le i \le g$$

here g is the number of internal nodes.

Each spline at any internal point of the interval between the neighboring nodes $x \in [\lambda_j, \lambda_{j+1}]$ was represented in a basic form as a recursive relation to the splines of the previous order [32]:

$$N_i^{k+1}(x) = \alpha_i^k(x) N_i^k(x) + \left(1 - \alpha_i^k(x)\right) N_{i+1}^k(x) \tag{2}$$

where

$$\alpha_i^k(x) = \begin{cases} \frac{x-\lambda_i}{\lambda_{i+k}-\lambda_i}, & \lambda_i \neq \lambda_{i+k} \\ 0. & \lambda_i = \lambda_{i+k} \end{cases} \tag{3}$$

and the first order splines, which are the starting points of the recursion, were given as a meander:

$$N_i^1(x) = \begin{cases} 1, & x \in [\lambda_i, \lambda_{i+1}[\\ 0, & x \notin [\lambda_i, \lambda_{i+1}[\end{cases} \tag{4}$$

To calculate the coefficients with the best approximating the initial noisy array of $\boldsymbol{n}$ experimental points, we found the minimum of functional:

$$\delta(c) = \sum_{i=0}^{n-1} \left[y_i - \sum_{j=0}^{g+k} c_j N_j^{k+1}(x_i) \right]^2 \tag{5}$$

or as a matrix:

$$\delta(c) = \|y - A \bullet c\|^2 \tag{6}$$

The minimum is reached when the gradient on coefficients for discrepancy (the sum of squares of deviations of calculated spline points from experimental ones) is equal to zero:

$$\nabla\delta(c) = 0 \tag{7}$$

We need to specify the operator $\langle \cdots, \cdots \rangle$ of the scalar product:

$$\langle N_i, N_j \rangle = \sum_{m=0}^{n-1} N_i^{k+1}(x_m) \bullet N_j^{k+1}(x_m) \tag{8a}$$

and

$$\langle N_i, y \rangle = \sum_{m=0}^{n-1} N_i^{k+1}(x_m) \bullet y_m \tag{8b}$$

Let's enter the designations

$$B = A^T A = \begin{pmatrix} \langle N_0, N_0 \rangle & \cdots & \langle N_0, N_{g+k} \rangle \\ \vdots & \ddots & \vdots \\ \langle N_{g+k}, N_0 \rangle & \cdots & \langle N_{g+k}, N_{g+k} \rangle \end{pmatrix} \tag{9}$$

$$R = A^T y = \begin{pmatrix} \langle N_0, y \rangle \\ \vdots \\ \langle N_{g+k}, y \rangle \end{pmatrix} \tag{10}$$

Now the matrix Eq. (7) and the whole problem are reduced to solving a multi-dimensional system of linear equations:

$$Bc = R \tag{11}$$

A characteristic feature of such problems is that matrix B turns out to be $(2\ k+1)$-diagonal because when $|i-j| > k$, the scalar product_ $\langle N_i, N_j \rangle = 0$. In this case, instead of standard system of linear algebraic equations (SLAE) methods, such as, for example, the Gauss method, it is more reasonable to use the Cholesky decomposition [33, 34].

To ensure not only the fitting of spline primary data, but also their smoothing, an additional requirement was introduced for minimizing outliers of derivatives of the spline polynomial up to the k-th order. This problem is also reduced to the SLAE solution by the Cholesky algorithm, and to avoid numerical errors in the source data was introduced a small perturbation—about 10^{-7} from the main signal. Taking into account the necessity of mass data preparation and also preprocessing and postprocessing, we have implemented the specified algorithm with minor changes to VBA-Excel environment, which is best suited for these purposes.

The number of N_y points in the experimental data array accepted for processing was varied from 190 to 550. The number of interpolation points N was usually taken as 250 and was strictly the same for all spectra within series and for different series as well. The B-spline order was limited to three due to the role of high-frequency beats rise markedly as it increased.

3 Results and Discussion

3.1 EPR Spectroscopy

EPR spectra of some prepared samples in the presence of air are shown in Fig. 1 presenting V–TiO_2 Hombikat UV100 nanoparticles after different times of incubation in 0.65 M of the ascorbic acid. $[VO^{2+}]$ content is $2.65 \cdot 10^{19}$ spin/g. One can see noticeable changes of the spectra (in low-field components related to the parallel orientation of PCs in the magnetic field and in the central component of the perpendicular orientation) in time of incubation. As it was revealed in [27], double integration of EPR spectra showed that the total concentration of PCs is not changing, in the precision of measurements during the whole time of the experiment. Changing of the spectrum shape reflects transformations occurring in the system under investigation. Paramagnetic vanadium ions exist on V-TiO_2 surface in two main forms: isolated and aggregated, and dynamics of their reorganization has been studied in [27] where it was found that vanadium PCs in both forms are represented by similar VO^{2+} species.

Figure 2 illustrates the behavior of vanadium species on the surface of V–TiO_2 particles for a long time of incubation. One can see that concentration of isolated PCs increases noticeably in time whole the content of aggregated species decreases. These dependences were obtained under experimental EPR spectra simulations using the computer program described in [29] and further double integration of the resulted simulated spectra. It was shown that at low $VOSO_4$ concentration VO^{2+} aggregates are not formed but they constitute a significant portion of the total

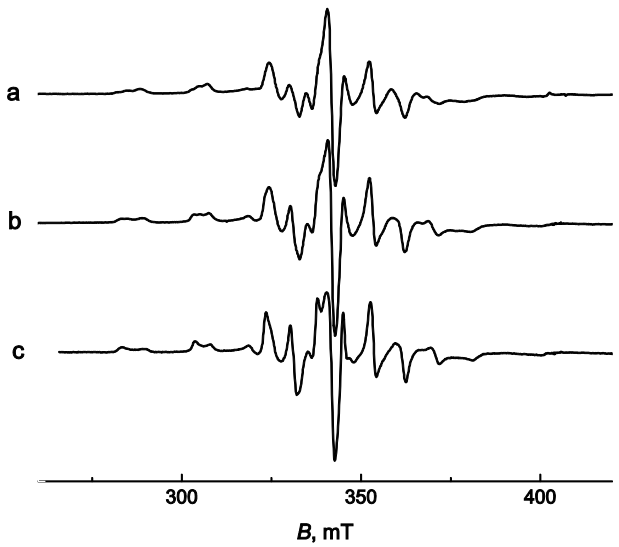

Fig. 1 EPR spectra at 77 K of V-TiO_2 Hombikat UV100 nanoparticles after 1 h (*a*), 15 days (*b*), and 54 days (*c*) of incubation in 0.65 M of the ascorbic acid. $[VO]^{2+}$ content is $5.5 \cdot 10^{19}$ spin/g

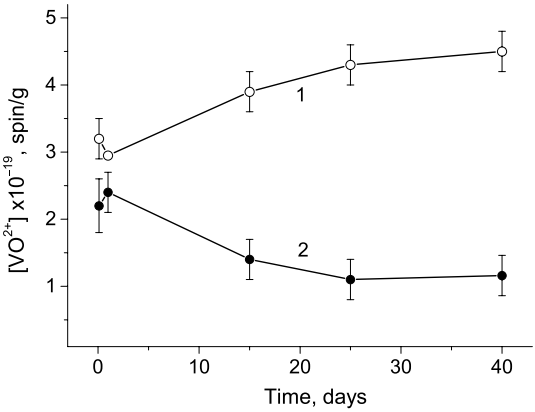

Fig. 2 Concentration of the isolated (*1*) and aggregated (*2*) VO^{2+} PCs formed on V–TiO_2 Hombikat UV100 surface as a function of the incubation time for a sample with $5.5{\cdot}10^{19}$ spin/g of total content of vanadium PCs

paramagnetic species at high $VOSO_4$ content and the part of the VO^{2+} aggregated PCs increases relating to the part of the isolated PCs [27].

The detailed analysis of low-field components (the parallel orientation of spins in the external magnetic field) of EPR spectra recorded at different times of incubation showed that these components are not individual but consist of three lines each designated as *A*, *B*, and *C*, with their amplitudes sufficiently changed in time (Fig. 3) which demonstrates this much more explicit in comparison with Fig. 1. Spin Hamiltonian values of these PCs were determining and listed in [27] but we would note that whose values could be not correct exactly because the spectral resolution of three last components of the parallel orientation are not fine enough to be sure of the real $g_{\|}$ and $A_{\|}$ data. We will return back to this problem below.

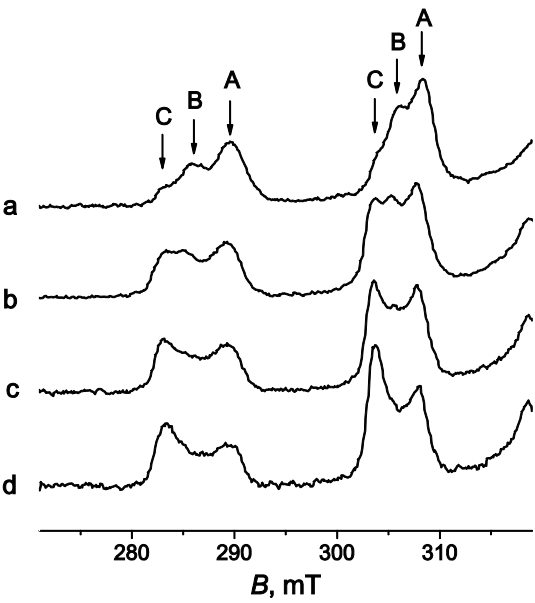

Fig. 3 Low-field lines of EPR spectra at 77 K of V-doped TiO_2 Hombikat UV100 particles with $[VO]^{2+}$ ($2.65{\cdot}10^{19}$ spin/g) after 1 h (*a*), 15 (*b*), 40 (*c*), and 54 days (*d*) of incubation. Letters *A*, *B* and *C* mark lines of three different VO^{2+} PCs on V–TiO_2 surface

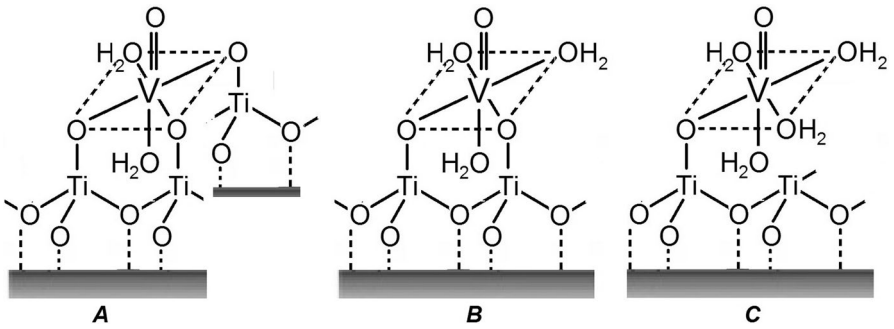

Fig. 4 Schematic structures of VO^{2+} complexes *A*, *B*, and *C* on the TiO_2 surface

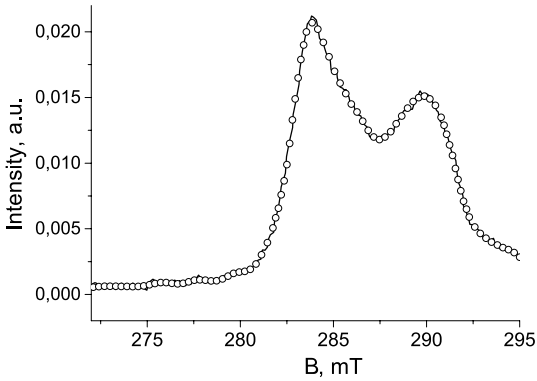

Fig. 5 Spline of primary data with 25 internal nodes. It seems to be an optimal number of nodes, the interpolation spectrum repeats only the experimental peaks, but filters out high-frequency noise

One can assume that paramagnetic species *A*, *B*, and *C* characterize VO^{2+} PCs with structures formed on the TiO_2 surface with different number of the Ti–O–V bonds and distortions of the spatial coordination sphere of the vanadium complex. It is known from the theory of EPR spectroscopy [28, 35, 36] that in the line of paramagnetic metal complexes with different numbers *n* of the same ligand atoms (O, N, S, etc.), the position of the first low-field component is usually shifted to the higher magnetic field *B* magnitudes with stronger interaction with the ligand atoms, *i.e.*, with the increase of the number *n* of coordinated atoms. According to this and to a fact that the intensity of lines (*C*) in Fig. 3 increases in time of incubation, and that of lines (*A*) decreases, there was suggested that lines (*A*), (*B*) and (*C*) belong to complexes with one, two and three Ti–O–V bonds in the coordination sphere of VO^{2+}–TiO_2 PCs. Figure 4 illustrates these structures schematically.

Transformations of the first low-field component of EPR spectra evidently seen in Fig. 3 has to be carefully analyzed for obtaining information about dynamics of changes and their quantitative description. The formal mathematical procedure of calculating such data from experimental spectra as well as the results obtained are presented in the next section. It became also possible to determine with much

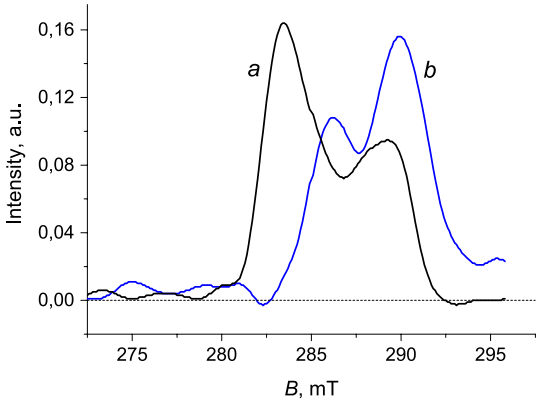

Fig. 6 Normalized base spectra with minimal «mutual presence»

higher precision the $g_{||}$ and $A_{||}$ values of various paramagnetic VO^{2+}-doped Hombikat UV 100 TiO_2 nanoparticles formed on the surface.

3.2 Kinetics and Transformations

Analysis of EPR spectra using interpolation by cubic splines showed that the best results are obtained in the range of $20 < g < 30$, where the quality of interpolation is least sensitive to the choice of the number of internal nodes. When the number of nodes is increased to 100, the spline reproduces not only the shape of the spectrum, but virtually all parasitic noise. Therefore, we have adopted $g = 25$ and $N = 250$ as the "internal standard", and thus we have processed arrays of 250 points from $H = 2700$ G to $H = 2949$ G with 1 G steps (Fig. 5).

After preprocessing the primary data and bringing it to a standardized format with 250 pixels, in the standardized range from $H = 2700$ to 2949 G, the data were transferred to a blind spectrum separation program that we prepared ourselves.

In the method of least squares Multivariate Curve Resolution (MCR) [37, 38], arrays of experimental data are rows of data matrix D (that's why on the previous step we had to bring the original data to the format of the same dimension). The task is to decompose D into the product of two smaller matrices C and S^T, where C is a one-dimensional matrix-column of concentration profiles. It is important to emphasize that the height of this column is unknown, i.e. we do not have a priori information on how many substances (initial, intermediate, and final) contribute to the recorded spectrum. Similarly, we do not know the reference spectra; we have to calculate matrix S, whose rows are the spectra of the corresponding pure individual (or assumed) components. Since we do not know the column height of concentrations, we do not know the number of rows in the spectrum matrix—both equal to the number of independent components. We know only the number of the reference matrix columns—the number of spectroscopic channels, which in our case are 250.

The processing procedure included determination of matrix D rank (number of linearly independent components in the system under study), finding of eigenvalues

and eigenvectors of matrix D, compilation of the basis of reference spectra, on which all experimental spectra can be decomposed. Further, normalization of the basis was performed to obtain the most probable combination of components and to extract kinetic information for each of the base components.

In the first step, a covariance matrix A was built, the elements of which are paired scalar products of experimental spectra:

$$\mathcal{A}_{ij} = \langle S_i, S_j \rangle \tag{12}$$

It is a square symmetrical matrix. The most direct and reliable way to calculate its rank is to determine the set of its own values by bringing the matrix to the normal form of Frobenius. For this purpose, the Danilevsky algorithm [39–41] was implemented.

The matrix is reduced to standard Frobenius form, each of the transfer matrix is calculated as the difference between the characteristic polynomials of two matrices which are related to the system state matrix, and the polynomials are computed by the method of Danilevsky, which is used in many numerically intensive calculations where extreme eigenvalues have to be estimated.

In the form of Frobenius in the matrix there are non-zero elements only on the first line and under the main diagonal, where they are equal to unit. This form is ideal for compiling a characteristic polynomial and defining eigenvalues. The polynomial coefficients are elementary obtained by decomposition of the matrix determinant in the first line:

$$\lambda^n - p_1\lambda^{n-1} - p_2(-\lambda)^{n-2} - \cdots - p_n = 0 \tag{13}$$

The search for the real roots of the polynomial equation is not fundamentally difficult. It was carried out using stable algorithm independent of heuristic operations on setting and selection of the starting approximation. The solution of the characteristic polynomial in all cases gave only two roots—eigenvalues, which corresponds to two independent components in mixed spectra, and indicates the absence of spectroscopically significant intermediate states.

Extracting the "true" spectra, we used an algorithm that consistently reduces the "mutual presence" of spectra and includes the following two procedures:

1. Successive output of all spectra to the positive region.
2. Sequential "abstraction" of common spectral lines so that ideally each line would be contained in only one base spectrum. In practice, it is not always possible to reduce to a base of the species "one line—one presence", but, as studies have shown, this is not necessary in practice. Consistent application of these two procedures gives rather good set of base spectra (Fig. 6).

The next step is to obtain kinetic curves for the initial substance and the final product, associated with the decomposition of spectra related to different time moments on the normalized basis. The basis of spectra from Fig. 6 shows that the "decomposition of components" did not occur completely. And instead of two pure exponential functions describing the drop in the fraction of isolated PCs of type A

from 1 to zero with the antibate increase in the fraction of VO^{2+} PCs of type *C* from 0 to 1, changes in the narrowed range from 0.34 to 0.66.

Formally, this corresponds to the fraction of isolated VO^{2+} centers in PCs *A* and *C* at the beginning and end of the experiment. To adjust the base spectra to the expected kinetics $A \rightarrow C$ for true fractions, the Moore–Penrose matrix [42, 43] must be used. After that, kinetic curves will be obtained, allowing determine the rate constant of transformation of isolated VO^{2+} centers of type *A* into type *C*. Figure 7 clearly demonstrates this.

One can see from Fig. 7 that three samples with different initial content of paramagnetic vanadium PCs reveal practically coincident kinetic behavior in the range of $2.65 \cdot 10^{19} \leq [VO^{2+}]_0 \leq 12.5 \cdot 10^{19}$ spin/g which can be characterized by the effective kinetic constant of the first order k_{-1} equal approximately to 0.14 – 0.15 $(day)^{-1}$. Results shown in Fig. 7 objectively demonstrate that transformations from *A* to *C* complexes occur irreversibly and are really first-order reactions relating to vanadium concentration. This follows from the exponential behavior of kinetic plots as well as from independence of the rate constant on the initial concentration of $[VO^{2+}]_0$.

One more fact has attracted our attention: the computer program which we used for determining EPR line positions and transformation kinetics has revealed only two basic states, *A* and *C*, of VO^{2+} PCs (Figs. 6, 7) while EPR spectra in Fig. 3 demonstrate evidently lines characterizing complex *B* at all times of incubation. We should note that computer analysis of the complete set of the experimental first low-field and the eighth high-field EPR components gave separately rather exact positions for all *A*, *B* and *C* centers. This contradiction can be caused by the approximately constant concentration of PCs *B* during the whole period of the experiment. In such a case, the program does not simply notice this intermediate but permanently existing species which are not the limiting factor of the transformation process.

This mathematical method became also useful for clarification of spin Hamiltonian parameters of VO^{2+} complexes. Indeed, high precision of determining line positions of *A*, *B*, and *C* paramagnetic species have increased accuracy of these measurements. Table 1 contains $g_{\|}$, $A_{\|}$ and $g_{\perp}$, $A_{\perp}$ values for these PCs calculated in this work in comparison with those published in Ref. [27]. One can see from the

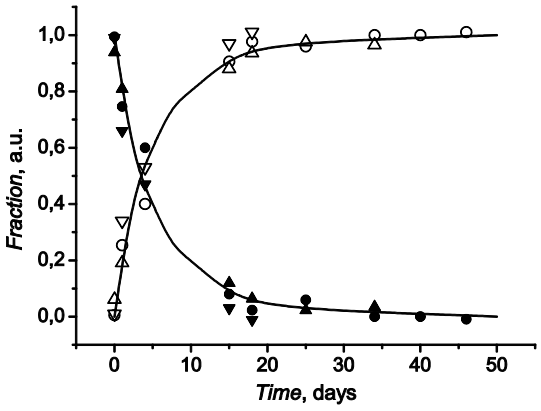

Fig. 7 Fractions of the components *A* (●, ▲, ▼) and *C* (○, Δ, ∇) shown in Fig. 2 as a function of the incubation time for samples with: $2.65 \cdot 10^{19}$ (●, ○), $8.7 \cdot 10^{19}$ (▲, Δ), and $12.5 \cdot 10^{19}$ spin/g (▼, ∇) of paramagnetic vanadium PCs

Table 1 EPR parameters of V-doped TiO_2 species at 77 K

Center	$A_{\|}$, mT	$g_{\|}$	$A_{\perp}$, mT	$g_{\perp} \pm 0.002$
VO^{2+}, *A*	17.86 ± 0.1	1.933 ± 0.001	–	–
VO^{2+}, *B*	18.76 ± 0.1	1.935 ± 0.001	–	–
VO^{2+}, C	19.51 ± 0.1	1.935 ± 0.001	–	–
VO^{2+}, A [27]	17.9 ± 0.2	1.931 ± 0.002	7.25	1.981
VO^{2+}, B [27]	19.1 ± 0.2	1.933 ± 0.002	–	–
VO^{2+}, C [27]	19.45 ± 0.2	1.935 ± 0.002	7.0	1.975
$VO(H_2O)_5^{2+}$ [27]	20.1 ± 0.2	1.933 ± 0.002	7.62	1.983
- "- [44]	20.5	1.931	7.7	1.978

Table that some values obtained in this work are a little bit different comparing to those given in [27] and more precise due to more objective analysis of the complete set of experimental EPR spectra and mathematical possibilities of the analytical method.

4 Conclusion

For the first time, EPR investigation of photocatalytic systems based on vanadium modified titanium dioxide (TiO_2, anatase) surface containing various concentrations of VO^{2+} paramagnetic centers allowed not only distinguishing but also quantitative characterizing three different types of the isolated PCs existing on the surface of V–TiO_2 nanoparticles. Special computer program has been developed for the precise identification of partially resolved EPR spectra and calculating kinetic parameters of time-dependent transitions between these PCs. This program allowed determining and describing structural behavior of these PCs which contain different number of the ligand oxygen atoms of the titania surface in VO^{2+} coordination sphere. Slow dynamics of the surface reorganization have been observed and resulted in calculating the kinetic rate constant equal to *ca*. 0.15 $(day)^{-1}$. Computer analysis of the low-field and high-field components of EPR spectra using new theoretical approach helped also to determine $g_{\|}$ and $A_{\|}$ of vanadium PCs with higher precision.

Acknowledgements This work was supported by the State assignment of RF № AAAA-A20-120021390044–2. We are thankful to Prof. A. Kh. Vorob'ev (Department of Chemistry, M. V. Lomonosov Moscow State University) provided us his computer Program package.

References

1. J.C.-S. Wu, C.-H. Chen, J. Photochem. Photobiol. A: Chemistry **163**, 509 (2004)
2. W.-F. Chen, P. Koshy, L. Adler, C.C. Sorrell, J. Austral. Ceram. Soc. **53**, 569 (2017)
3. S. Liu, T. Xie, Z. Chen, J. Wu, Appl. Surface Sci. **255**, 8587 (2009)
4. M. Bettinelli, V. Dallacasa, D. Falcomer, P. Fornasiero, V. Gombac, T. Montini, L. Romano, A. Speghini, J. Hazard. Mater. **146**, 529 (2007)
5. H. Khan, D. Berk, J. Sol-Gel Sci. Technol. **68**, 180 (2013)
6. I. Cimieria, H. Poelmanb, J. Ryckaerta, D. Poelman, J. Photochem. Photobiol. A: Chem. **263**, 1 (2013)
7. S. Klosek, D. Raftery, J. Phys. Chem. B **105**, 2815 (2001)

8. K. Bhattacharyya, S. Varma, A.K. Tripathi, S.R. Bharadwaj, A.K. Tyagi, J. Phys. Chem. C **112**, 19102 (2008)
9. J. Zhou, M. Takeuchi, A.K. Ray, M. Anpo, X.S. Zhao, J. Coll. Interface Sci. **311**, 497 (2007)
10. S.T. Martin, C.L. Morrison, M.R. Hoffmann, J. Phys. Chem. **98**, 13695 (1994)
11. M. Pérez-Nicolás, I. Navarro-Blasco, J.M. Fernández, J.I. Alvarez, Construct. Build. Mater. **149**, 257 (2017)
12. G. Rossi, L. Pasquini, D. Catone, A. Piccioni, N. Patelli, A. Paladini, A. Molinari, S. Caramori, P. O'Keeffe, F. Boscherini, Appl. Catal. B: Environ. **237**, 603 (2018)
13. J. Shyue, M.R. De Guire, J. Am. Chem. Soc. **127**, 12736 (2005)
14. E. Roncari, C. Galassi, S. Ardizzone, C.L. Bianchi, Colloids Surf. A: Physicochem. Eng. Aspects **117**, 267 (1996)
15. S. Youn, S. Jeong, D.H. Kim, Catal. Today **232**, 185 (2014)
16. G. Busca, L. Marchetti, J. Chem. Soc. Faraday Trans. **81**, 1003 (1985)
17. G. Deo, I.E. Wachs, J. Catal. **146**, 335 (1994)
18. K. Nagase, Y. Shimizu, N. Miura, N. Yamazoe, Appl. Phys. Lett. **61**, 243 (1992)
19. T. Ivanova, A. Harizanova, Mater. Res. Bull. **40**, 411 (2005)
20. S. Songara, M.K. Patra, M. Manoth, L. Saini, V. Gupta, G.S. Gowd, S.R. Vadera, N. Kumar, J. Photochem. Photobiol. A: Chem. **209**, 68 (2010)
21. Z.M. Tian, S.L. Yuan, S.Y. Yin, S.Q. Zhang, H.Y. Xie, J.H. Miao, Y.Q. Wang, J.H. He, J.Q. Li, J. Magn. Magn. Mater. **320**, L5 (2008)
22. J.H. Chang, Y.L. Wang, C.D. Dong, S.Y. Shen, Catalysts **10**, 482 (2020)
23. T. Wu, W. Kong, Y. Zhang, Z. Xing, J. Zhao, T. Wang, X. Shi, Y. Luo, X. Sun, Small Methods **3**, 1900356 (2019)
24. D.P. Opra, S.V. Gnedenkov, A.A. Sokolov, A.B. Podgorbunsky, A.Y. Ustinov, V.Y. Mayorov, V.G. Kuryavyi, S.L. Sinebryukhov, J. Mater. Sci. Technol. doi: 10.1016/j.jmst.2020.02.068 (2020)
25. H. Seo, D. Ichida, S. Hashimoto, N. Itagaki, K. Koga, M. Shiratani, S.-H. Nam, J.-H. Boo, J. Nanosci. Nanotechnol. **16**, 4875 (2016)
26. M. Crisan, M. Zaharescu, D. Crisan, R. Ion, M. Manolache, J. Sol-Gel Sci. Technol. **13**, 775 (1998)
27. A.I. Kokorin, V.I. Pergushov, A.I. Kulak, Catal. Lett. **150**, 263 (2020)
28. H.A. Kuska, M.T. Rogers, *ESR of First Row Transition Metal Complex Ions* (Wiley, New York, 1968)
29. A. Kh. Vorob'ev, N.A. Chumakova, in *Nitroxides: Theory, Experiment and Applications*, ed. by A.I. Kokorin (InTech Publ., Rijeka, 2012), pp. 57–112
30. M.G. Cox, J. Inst. Maths. Appl. **15**, 95 (1975)
31. C. de Boor, J. Approx. Theory **6**, 50 (1972)
32. K. Lee, *Principles of CAD/CAM/CAE Systems* (Addison-Wesley, Reading, MA, 1999)
33. W.H. Press, S.A. Teukolsky, W.T. Vetterling, B.P. Flannery, *Cholesky Decomposition, Numerical recipes 3rd edition: The art of scientific computing* (Cambridge Univ. Cambridge, Cambridge, 2007)
34. B.S. Andersen, J.A. Gunnels, F.G. Gustavson, J.K. Reid, J. Waśniewski, A.C.M. Transact. Math. Softw. **31**, 201 (2005)
35. S.A. Al'tshuler, B.M. Kozyrev, *Electron Paramagnetic resonance of the Compounds of Intermediate Groups* (Nauka, Moscow, 1972). **(in Russian)**
36. A. Carrington, A.D. McLachlan, *Introduction to Magnetic Resonance with Applications to Chemistry and Chemical Physics* (Harper & Row, New York, 1967)
37. Yu.B. Monakhova, S.A. Astakhov, A.I. Kraskov, S.P. Mushtakova, Chemomet. Intel. Labor. Systems **103**, 108 (2010)
38. H. Parastar, M. Jalali-Heravi, R. Tauler, Trends Anal. Chem. **31**, 134 (2012)
39. D.K. Faddeev, V.N. Faddeeva, *Computational Methods of Linear Algebra* (Mathematics Series. Freeman, San Francisco, 1963)
40. V.M. Verzhbitskiy, *Fundamentals of Numerical Methods* (Vysshaya shkola, Moscow, 2002)
41. K.K. Appukuttan, S. Bhat, J. Control Sci. Eng. doi: 10.1155/2010/789404 (2010)
42. P. Courrieu, Neural Inform. Proc. Lett. Rev. **8**, 25 (2005)
43. J.C.A. Barata, M.S. Hussein, Brazil. J. Phys. **42**, 146 (2012)
44. V. Luca, S. Thomson, R.F. Howe, J. Chem. Soc., Faraday Trans. **93**, 2195 (1997)